*energies*

MDPI

*Article*

# Modified Cascaded Controller Design Constructed on Fractional Operator 'β' to Mitigate Frequency Fluctuations for Sustainable Operation of Power Systems

**Muhammad Majid Gulzar [1], Sadia Murawwat [2], Daud Sibtain [3], Kamal Shahid [4], Imran Javed [5] and Yonghao Gui [6,*]**

[1] Control & Instrumentation Engineering Department, King Fahd University of Petroleum & Minerals, Dhahran 31261, Saudi Arabia
[2] Department of Electrical Engineering, Lahore College for Women University, Lahore 54000, Pakistan
[3] Department of Electrical Engineering, University of Central Punjab, Lahore 54000, Pakistan
[4] Institute of Electrical, Electronics and Computer Engineering, University of the Punjab, Lahore 54590, Pakistan
[5] Department of Electrical Engineering, Narowal Campus, University of Engineering and Technology Lahore, Narowal 39161, Pakistan
[6] Department of Electronic Systems, Aalborg University, 9220 Aalborg, Denmark
* Correspondence: guiy@ornl.gov

**Abstract:** The demand for energy is increasing at an abrupt pace, which has highly strained the power system, especially with high share of power generation from renewable energy sources (RES). This increasing strain needs to be effectively managed for a continuous and smooth operation of the power system network. Generation and demand exhibit a strong correlation that directly creates an impact on the power system frequency. Fluctuations and disruptions in load frequency can manifest themselves as over-voltages and physical damages in the power grid and, in the worst case, can lead to blackouts. Thus, this paper proposed an effective solution to mitigate the load frequency problem(s), which is initiated by the changing load demand under high penetration of RES. This paper presented an improved cascaded structure, the proportional integral with a fractional operator coupled with proportional derivative $(PI - (FO_P + PD))$. The proposed $FO_P + PD$ modifies the (1+PD) controller by introducing fractional properties that improve its tracking efficiency and mitigate frequency fluctuations taking minimal time. The introduction of $FO_P$ $(\beta)$ diversifies its tracking and overall controlling ability, which translates it as a significant controller. The controller optimal parameters are extracted by deploying a dragonfly search algorithm (DSA). The study of the results illustrates that the proposed design displays efficient performance under any disturbance or uncertainty in the power system.

**Keywords:** load frequency control; modified cascade controller; dragonfly search algorithm; fractional operator; renewable energy resources



**Citation:** Gulzar, M.M.; Murawwat, S.; Sibtain, D.; Shahid, K.; Javed, I.; Gui, Y. Modified Cascaded Controller Design Constructed on Fractional Operator 'β' to Mitigate Frequency Fluctuations for Sustainable Operation of Power Systems. *Energies* **2022**, *15*, 7814. https://doi.org/10.3390/en15207814

Academic Editor: Ahmed Abu-Siada

Received: 17 September 2022
Accepted: 18 October 2022
Published: 21 October 2022



## 1. Introduction

In the desire to handle the soaring challenges of the power system, the advancement in technology is very crucial. Sustainable energy growth has been a need of the hour for progressive development in the power sector. Environment-friendly power production is always a major concern; nowadays, to extract energy from natural sources, a dramatic shift has been devoted toward renewable energy resources (RES) such as photovoltaic (PV), wind, hydro, geothermal, etc. [1–3]. Consequently, the impact of RES is conspicuous on the energy generation; however, these RES enforce several challenges on the power system that result in stability issue [4,5]. In addition, the mismatch in generation and demand engenders stability issue, which affects the frequency of the power system (mainly on a frequency regulatory unit). The frequency disruption can be restored to its nominal operation by load frequency

control (LFC) [6]. The paper [7] emphasized the need for improved LFC design in complex power system contexts and a complete examination of numerous LFC structures in a variety of power system topologies, including single-area, multi-area, and multistage configurations. The authors of [8] proposed a method for mitigating low-frequency oscillations in power systems through the optimal technique of a power system stabilizer using an Ant-Lion optimization algorithm, and compared this method with existing conventional systems in order to achieve greater efficiency under a variety of load levels.

The major theme of LFC is to preserve the demand and generation synchronization to maintain the frequency within limits for a successful operation of the hybrid interconnected energy system. To counter such challenges of the power system, several articles have devoted their research on an efficient design of the control system to restrain frequency. Designing an efficient controller is always in focus to encounter the aforementioned challenges of the power system. Moreover, the microgrid stability is preserved by maintaining a zero steady-state error by the controller [9,10]. Considering the wake effect in a wind power plant, a coordinated wind power plant control for frequency support has been proposed in [11]. A data management functionality that enables data-driven update of settings and constraints (such as voltage, frequency, etc.) of the technique behind smart grid applications has been proposed in [12]. In order to support online frequency control from renewable power stations, an evaluation of the influence of communication and the associated factors has been presented in [13]. The authors of [13] also provided the relevance of the transmission system operator insights, and several communication factors such as infrastructure for general service communication and collaboration between wind power plants (WPPs), specifically primary frequency control management from WPPs for future power systems. Similarly, the study in [14] provided a distributed coordination technique using inverter-based resources to improve the running costs of microgrid systems, where the control strategy is proven to achieve optimum process and frequency even in the presence of communication failures. Multiple hierarchical techniques to power system control for single or multi-area microgrids have been recently developed. Typically, the proportional integral (PI)/proportional integral derivative (PID) controller for interconnected power grids is developed with high penetration RES in consideration [15,16].

A firefly algorithm (FA) and a genetic algorithm (GA) are used as optimizing algorithms to obtain optimum parameters for the PI controller; these controllers are deployed on a PV connected thermal system; however, it has shown sluggish reaction in achieving steady-state response [17]. Other evolutionary controllers such as particle swarm optimization (PSO) [18], cuckoo search (CS) technique [19], ant colony optimization (ACO) [20], and butterfly algorithmic technique implementation for LFC are deployed for optimizing the parameters required by the controller for its optimal operation [21].

Moreover, different development of PI/PID controllers is constructed to mitigate the effect of frequency fluctuation. Modified cascaded controllers are developed in order to improve the efficiency of the existing controllers. In a cascaded controller design, the effectiveness of the controller is improved by using a flower pollination algorithm (FPA), and to control the operation under a certain load change [22], hybrid stochastic fractal search and pattern search (hSFS-PS) [23], bat algorithm (BA) [24], and sine–cosine [25] tuned PI-PD controllers are designed. The cascaded structure PID+DD is developed, which utilizes the property of the multiverse optimizing technique for an interconnected hybrid system [26].

The PI-(1+PD) controller is applied with the help of a grasshopper optimizing algorithm (GOA) for the maritime microgrid [27]. Moreover, a fractional-order PID controller is enhanced by utilizing the dragonfly method to obtain optimal controller values, hence enhancing the controller's control operation [28]. The FOPID controller for automatic generation control (AGC) is implemented for multi-area power systems [29]. Another modified form of FOPI-FOPD is used to resolve the LFC problem, and the reliability of the cascaded controller is enhanced with the help of DSA [30].

In light of the aforementioned discussion, the response of the controllers suggests that there is a room for improvement in the cascade structure, which can further enhance the controlling ability of the cascaded design. Moreover, under high complexity, the effective

functioning of the power system is essential, and for this reason, the optimal operation of the controller is required to handle the rising problems posed by interconnected power systems.

*Novelty and Contribution*

In view of the literature review, certain sections can be identified that require further improvement, and the proposed methodology has invested its utility in the same direction to improve the ability of the cascaded design. The inspiration of this work is as follows:

1. The aim of the proposed research was to improve the ability of the existing cascaded controller to highlight rapid response under load perturbation to deal with frequency fluctuations.
2. The existing cascaded controller design PI-(1+PD) is modified to improve its efficiency. In PI-(1+PD), the factor one (1) is altered in the proposed design to achieve fast convergence. The factor one (1) in PI-(1+PD) is translated in terms of a fractional operator based on the input signal that helps to expedite the controller performance with low complexity. The tunable parameters of the proposed controller are extracted from DSA, and the proposed controller design is translated as PI-(FO_P+PD).
3. The testation of the proposed controller is scrutinized keeping a high penetration level of RES along with the energy storage system (ESS), where comparative performance assessment is evaluated through state-of-the-art control techniques.

The outcome and substantial contributions of this work are given below:

1. Developing a multi-area hybrid interconnected area including PV, wind, flywheel, battery ESS, and thermal system.
2. Hierarchy for PI-(FO_P+PD) is designed to counter the LFC problem.
3. The proposed controller is investigated by applying changing load and time delay in the power system.
4. The optimum parameters for the PI-(FO_P+PD) controller are extracted from DSA.

The paper is organized as follows. Section 2 provides the design and modeling of the PV, wind, thermal systems, and ESS. Section 3 provides details about the design of the PI-(FO_P+PD)-based controller. Section 4 describes the obtained results and discussions. Finally, Section 5 is dedicated for the conclusion and future work.

## 2. System Modeling

An interconnected two-area model is implemented to investigate the efficiency of a suggested controller. The model includes photovoltaic, wind, and thermal power plants, as well as a centralized ESS grid system. Each region consists of photovoltaic, wind, thermal power plant, and an ESS. Figure 1 illustrates the microgrid concept with interconnections. Each particular power plant system is described in depth in the previous subsections.

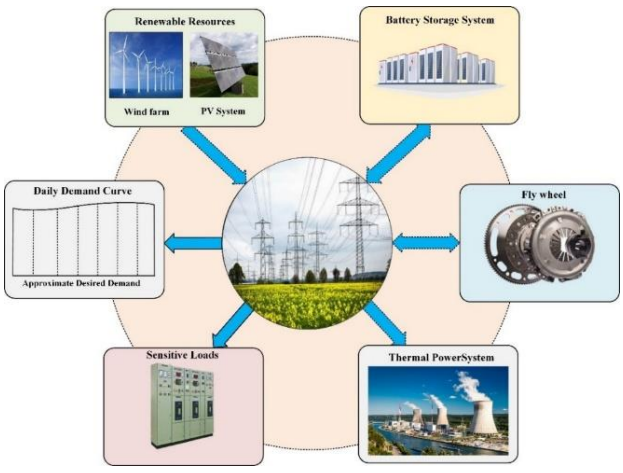


**Figure 1.** Overview of the system.

### *2.1. Thermal System Design*

The thermal system contains a turbine governor that collectively converts the energy into a mechanical rotation. The thermal unit plays a key part in deciding the overall system frequency due to its rotating component and its major impact in the power system. The variance in the generator speed is governed by the droop, which directly controls the prime mover [31]. The governor output power $\Delta P_{gi}(s)$, which is the difference of frequency change and reference power change, is specified in Equation (1):

$$\Delta P_{gi}(s) = \Delta P_{ref}(s) - \frac{1}{R}\Delta f_i(s) \tag{1}$$

where $\frac{1}{R}$ denotes the droop. The governor transfer function is given by [32]

$$G(s)_{Gov} = \frac{1}{T_g s + 1} \tag{2}$$

where $T_g$ is the time of governor constant. Similarly, the turbine transfer function can be written as (3) [28]

$$G(s)_{turbine} = \frac{1}{T_t s + 1} \tag{3}$$

In Equation (4), the ACE is enunciated as

$$ACE_i = B_i \Delta f_i + \Delta P_{tie\ ij} \quad i \neq j \tag{4}$$

$B_i$ denotes the frequency bias factor parameter.
$G_p(s) = \frac{1}{M_i s + D_i}$ is the generator output.

### *2.2. Photovoltaic Model*

The increasing trend of renewable energy sources cannot be ignored, especially that of the photovoltaic (PV). The transfer function for the PV model is given by (5) [33]:

$$Gpv(s) = \frac{\Delta P_{PV}(s)}{\Delta P_P(s)} = \frac{K_{PV}}{T_{PV} s + 1} \tag{5}$$

$T_{PV}$ and $K_{PV}$ signify the PV time and gain constant, respectively.

### *2.3. Wind Turbine Generator Model*

The perforation of wind energy into the grid further deteriorates the frequency. The modeling and designing of the wind turbine generator (WTG) for LFC issue are carried out [32]. The wind power system design is summarized as a transfer function in Equation (6):

$$G_{WT}(s) = \frac{\Delta P_{WT}(s)}{\Delta P_w(s)} = \frac{K_{WT}}{T_{WT} s + 1} \tag{6}$$

where $K_{WT}$ is the WT output gain constant, and $T_{WT}$ is the WT time constant equal to the change from the output power to input power.

### *2.4. Battery Energy Storage System*

The transfer function for the BESS can be attained from [33] and is given as Equation (7):

$$G_{BESS}(s) = \frac{\Delta P_{BESS}(s)}{\Delta P_{BE}(s)} = \frac{K_{BESS}}{T_{(BESS)} s + 1} \tag{7}$$

where $T_{BESS}$ is the BESS time constant, and $K_{BESS}$ is the BESS gain constant.

### *2.5. Flywheel for Energy Storage System*

The transfer function for the FESS can be extracted from [33] and is given in Equation (8):

$$G_{FESS}(s) = \frac{\Delta P_{FESS}(s)}{\Delta P_{FE}(s)} = \frac{1}{T_{(FESS)}s + 1} \tag{8}$$

where $T_{FESS}$ is the FESS time constant. The discussed system is summarized in Figure 2 from where the complete idea can be visualized.

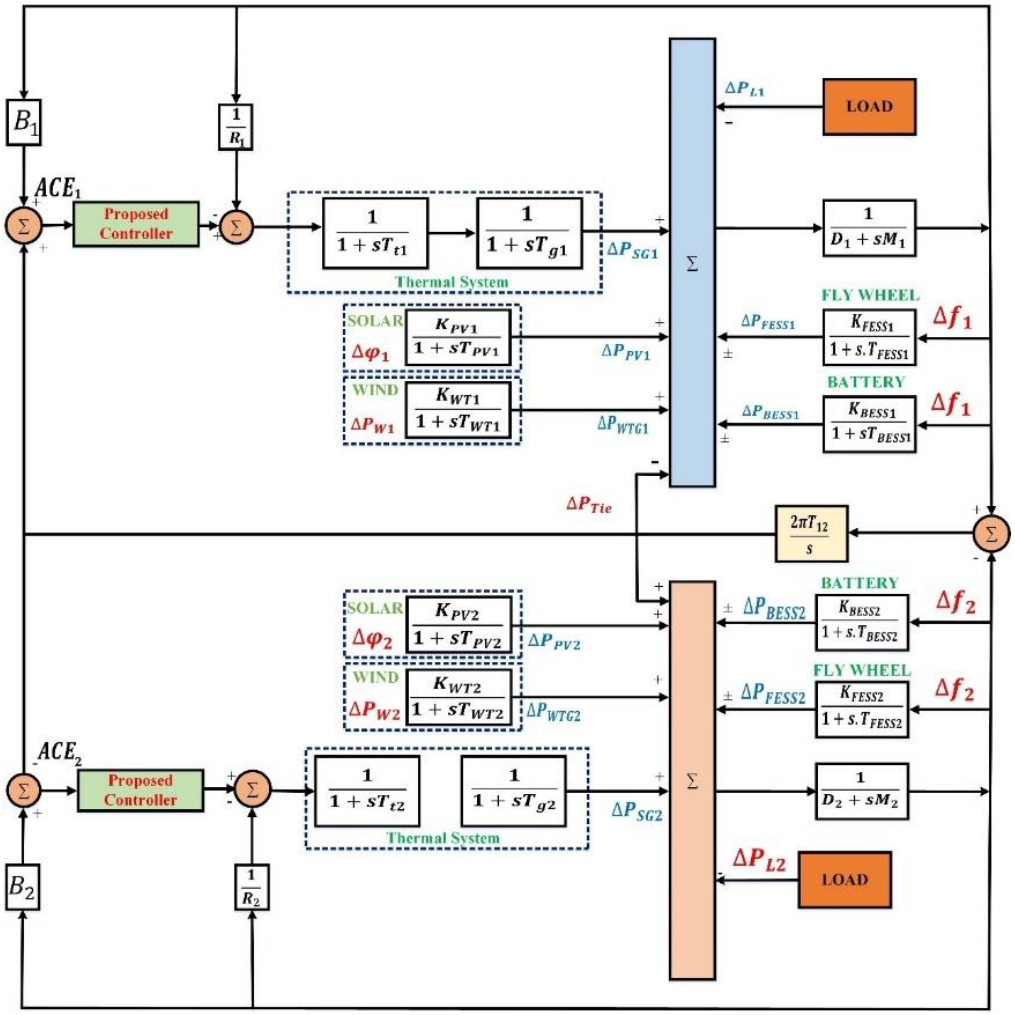


**Figure 2.** Model under study.

## 3. Proposed Cascaded Design

The proposed cascade structure proportional integral combined with fractional operator sums with proportional derivative (PI-(FO$_P$+PD)) is showcased in Figure 3. The design is an advanced form of (PI-(1+PD)) that modifies the (1+PD) part of the cascaded controller. The modified design helps to counter the LFC problem that generates due to the divergence in load and generation. In the proposed controller, the tunable parameters are optimized with the help of the dragonfly search algorithm (DSA) that generates optimal parameters for the proposed controller. The comparison analysis justifies the modified controller's effectiveness under various load scenarios.

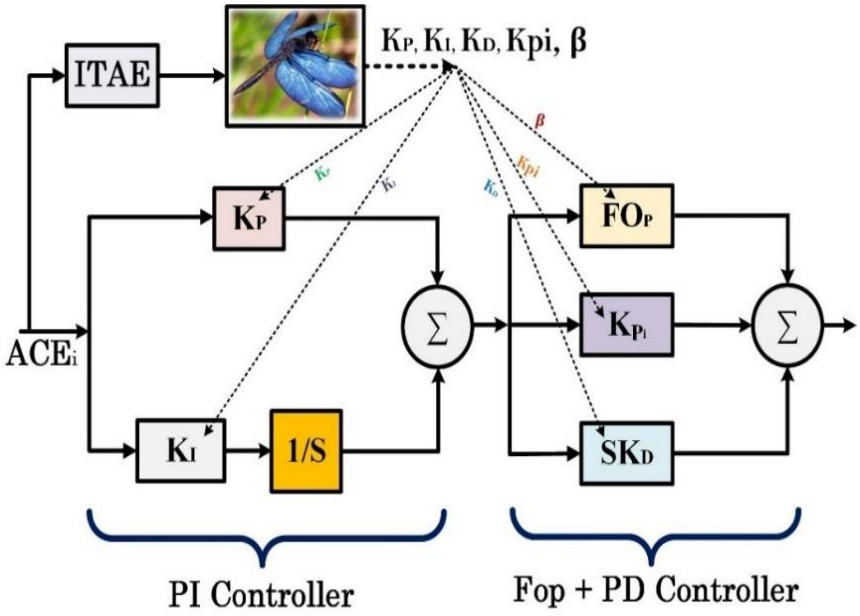


**Figure 3.** Proposed controller topology.

The controller expression for the output can be written as

$$\text{output} = \left(K_p + \frac{K_I}{s}\right) \times \left(s^{\beta} + K_{Pi} + sK_D\right) \tag{9}$$

where $K_p$, $K_I$, $\beta$, $K_{Pi}$, and $K_D$ represent the proportional gain, integral gain, operational factor, proportional gain for stage two, and derivative gain, respectively.

The expression of the ITAE for the two-area power system is shown in Equation (10):

$$\text{ITAE} = \int_0^{\infty} t(|\Delta f_1| + |\Delta f_2| + |\Delta P_{tie}|)dt \tag{10}$$

The ITAE is the objective function utilized for the algorithm to minimize it. $\Delta f_1$, $\Delta f_2$, and $\Delta P_{tie}$ are the change in frequency in area-1, change in frequency in area-2, and tie-line power change between the two areas.

The DSA is used to minimize the $J_s$ in the equation subject to (3):

$$\begin{cases} K_P^{min} \le K_P \le K_P^{max} \\ K_{Pi}^{min} \le K_{Pi} \le K_{Pi}^{max} \\ K_I^{min} \le K_I \le K_I^{max} \\ K_D^{min} \le K_D \le K_D^{max} \\ \beta^{min} \le \beta \le \beta^{max} \end{cases} \tag{11}$$

The range of gains for the proposed controller is between 0 and $-8$, whereas the $\beta$ parameter is set in between 0 and 1 for the proposed controller.

*Dragonfly Search Algorithm*

The dragonfly search algorithm (DSF) is a stochastic-based search algorithm that was proposed by Seyedali [33]. As the name implies, the DSF searches food and elusion from enemies. Dragonflies exist in nymph mostly for their lifetime, and then they switch their adult lives by metamorphosis. An image of a real dragonfly is shown in Figure 4 from where the idea of dragonfly can be conceived.

**Figure 4.** Real dragonfly.

The intelligence design is constructed on the basis of five factors: (1) separation, (2) alignment, (3) cohesion, (4) desire for food, and (5) distraction from enemy. The separation phenomenon is illustrated in Equation (12):

$$S_i = -\sum_{j=1}^{N} X - X_j \tag{12}$$

where $X - X_j$ defines the current position of an individual and the $j^{th}$ individual in the closing. N is the number of individuals in the field. The second factor alignment comes through Equation (13):

$$A_i = \frac{\sum_{j=1}^{N} V_j}{N} \tag{13}$$

Furthermore, the expression for cohesion can be achieved using Equation (14):

$$C_i = \frac{\sum_{j=1}^{N} X_j}{N} - X \tag{14}$$

Extraction of food and distraction from enemy are modeled in Equations (15) and (16), respectively.

$$F_i = X^+ - X \tag{15}$$

$$E_i = X^- + X \tag{16}$$

In Equations (15) and (16), $X^+$ and $X^-$ define the position of food source and position of enemy. The position of dragonflies is updated by Equation (17):

$$X_{t+1} = X_t + \Delta X_{t+1} \tag{17}$$

The step vector described in Equation (16) is similar to the velocity factor in PSO:

$$\Delta X_{t+1} = (sS_i + aA_i + cC_i + fF_i + eE_i) + w\Delta X_t \tag{18}$$

where s, a, c, f, and e are the swarming factors that form the swarming behavior of a dragonfly. If there is no closing dragonfly, the DSA can use Levy flight in a search space for a random and stochastic walk. If this case happens, the position is illustrated as

$$X_{t+1} = X_t + \text{Levy}(d) \cdot X_t \tag{19}$$

where d denotes the dimension of position vectors, and the function Levy (.) is calculated as Equation (20):

$$\text{Levy}(d) = 0.01 \cdot \frac{r_1 \cdot \sigma}{|r_2|^{\frac{1}{\beta}}} \tag{20}$$

$r_1$, $r_2$ are randomly generated, and their value lies in the range [0, 1]; β is a constant equal to 1.5, and σ is a variable. The utilization of the DSA is due to its simple and easy operations for implementation and required few control parameters, and it is found that the DSA deals better between the exploration and exploitation concept than its peers. The comprehensive detail procedure to extract controller gains is represented in Figure 5. The desired five parameters are optimized for the proposed controller, so the dragonfly is stated as

$$\text{dragonfly} = [K_P,\ K_I,\ K_D,\ Kpi,\ \beta] \tag{21}$$

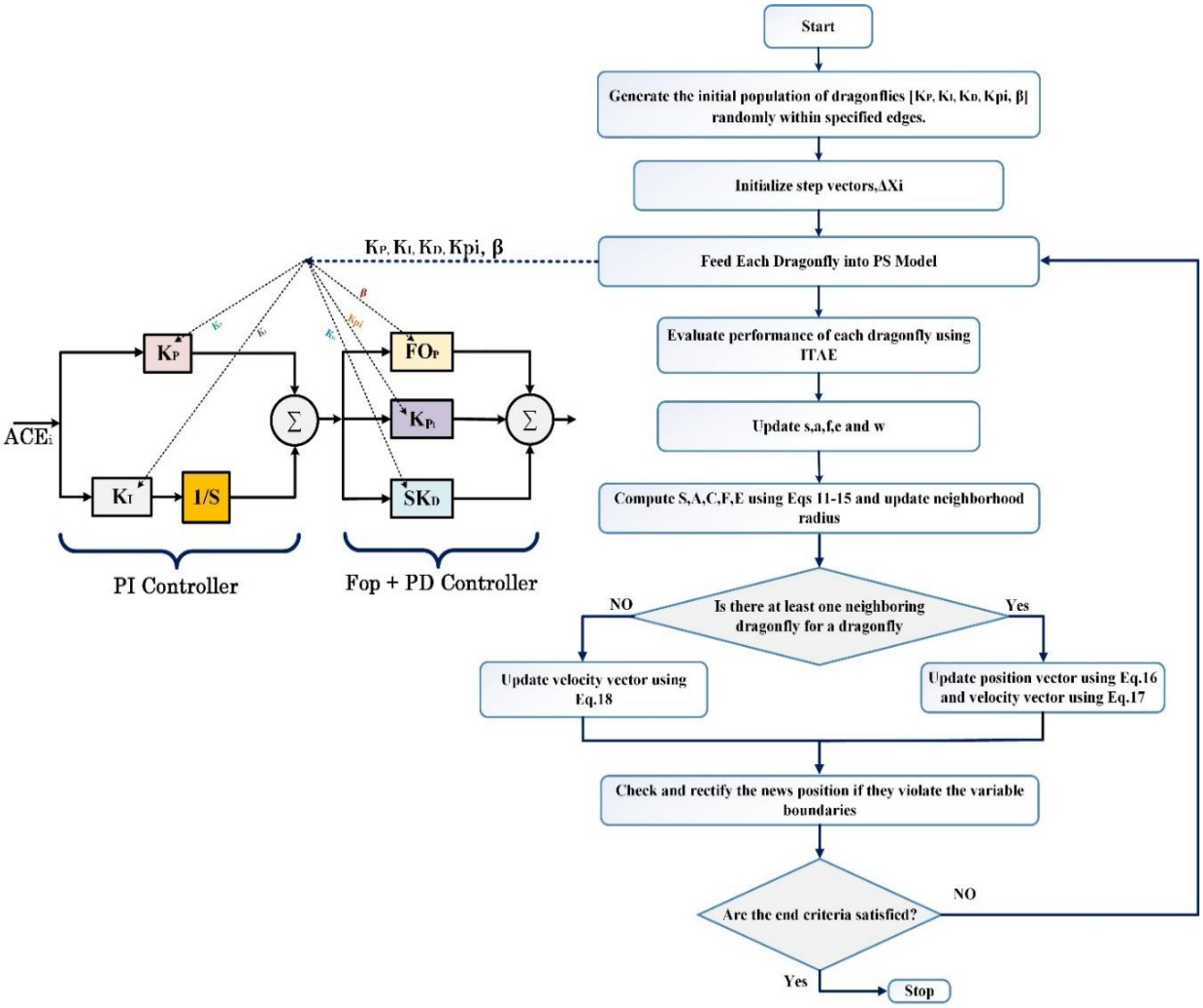


**Figure 5.** Flowchart of DSA.

The initializing parameters of the DSA are defined in Table 1.

**Table 1.** DSA initializing parameters.

| DSA | |
|---|---|
| Max-iteration | 100 |
| Dragonflies population (X) | 20 |
| Step vector (ΔX) | 10 |

The parameter values for various controllers are demonstrated in Table 2.

**Table 2.** Controllers' parameters after 100 iterations.

| Controller Parameters | FA−PI [7] | GWO: PI−PD [19] | DSA−FOPID [20] | Proposed Controller |
|---|---|---|---|---|
| Area-1 | $K_P = -0.5821$<br>$K_I = -0.8179$ | $K_{P1} = -2.8771$<br>$K_I = -2.7874$<br>$K_{P2} = -3.004$<br>$K_D = -2.0146$ | $K_P = 2.09$<br>$K_I = 4.344$<br>$K_D = 1.1487$<br>$\lambda = 0.988$<br>$\mu = 0.81$ | $K_{P1} = -4.98$<br>$K_I = -5.812$<br>$K_{P2} = -1.805$<br>$K_D = -1.215$<br>$\beta = 0.75$ |
| Area-2 | $K_P = -0.8869$<br>$K_I = -0.7257$ | $K_{P1} = -4.2809$<br>$K_I = -2.0014$<br>$K_{P2} = -2.9084$<br>$K_D = -1.2979$ | $K_P = 2.32$<br>$K_I = 4.941$<br>$K_D = 1.910$<br>$\lambda = 0.983$<br>$\mu = 0.80$ | $K_{P1} = -3.178$<br>$K_I = -6.847$<br>$K_{P2} = -0.580$<br>$K_D = -0.23$<br>$\beta = 0.77$ |

## 4. Results and Discussion

The proposed (DSA: PI-(FOp+PD) is tested under step load changes of 1% and 2.5%. Initially, the effectiveness of the proposed technique is verified under 1% load change for area-1 and area-2 as displayed in Figures 6 and 7, where the (DSA: PI-(FOp+PD) controller mitigates the frequency fluctuation in less than 4 sec when analyzed with other controllers. The distribution of power between interconnected areas is presented in Figure 8. From the result, it is evident that the controller with high efficiency can handle the power sharing in a more robust way.

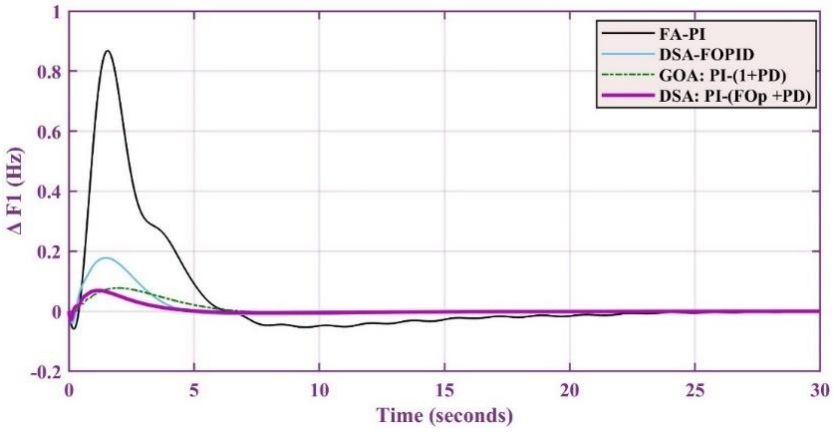


**Figure 6.** Response at 1% load change for area-1.

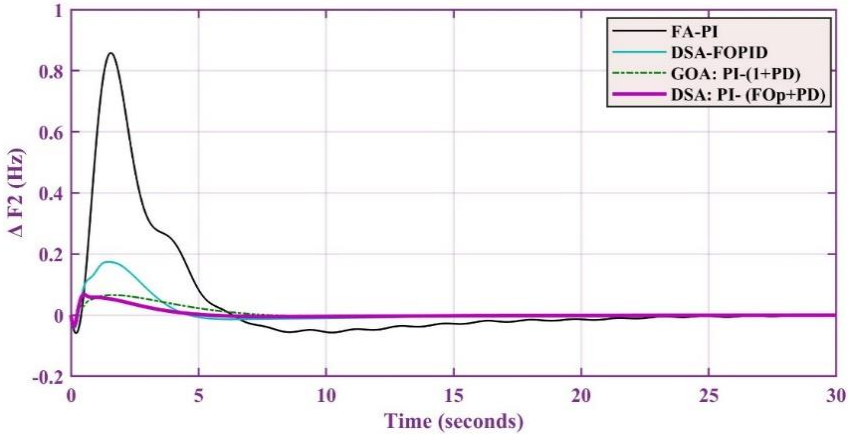


**Figure 7.** Response at 1% load change for area-2.

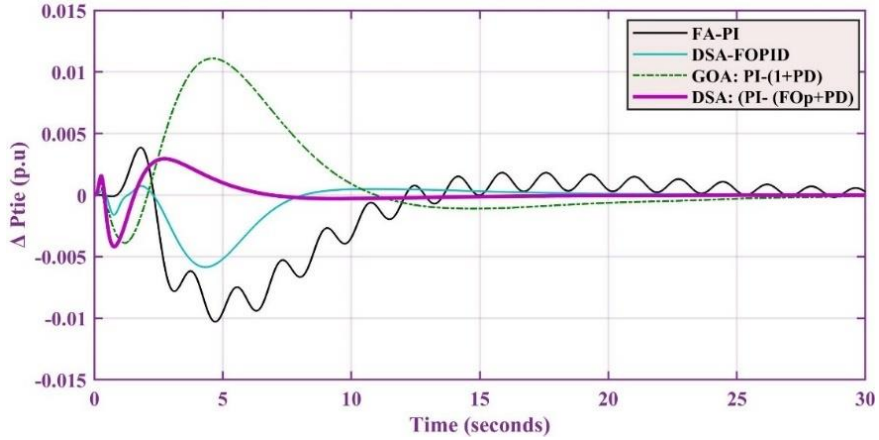


**Figure 8.** Tie-line power exchange response at 1% load change.

Correspondingly, the competency of Figures 9 and 10 exhibit the frequency response of the multi-area controller when subjected to a 2.5% load shift, whereas Figure 11 depicts the power exchange between the areas. The suggested controller outperforms conventional techniques in terms of rapid settling time and minimal oscillations.

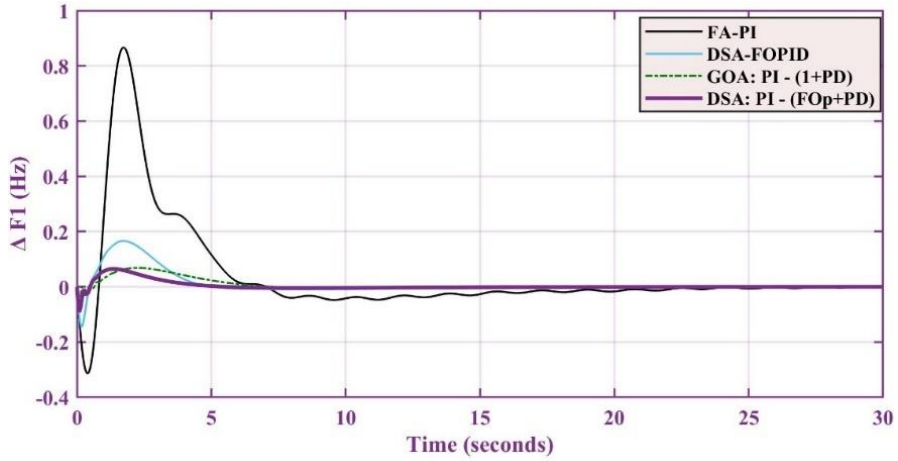


**Figure 9.** Response at 2.5% load change for area-1.

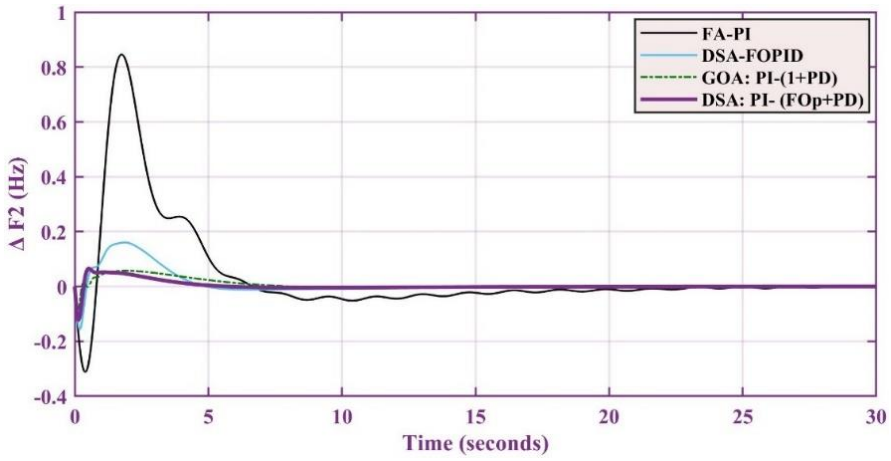


**Figure 10.** Response at 2.5% load change at area-2.

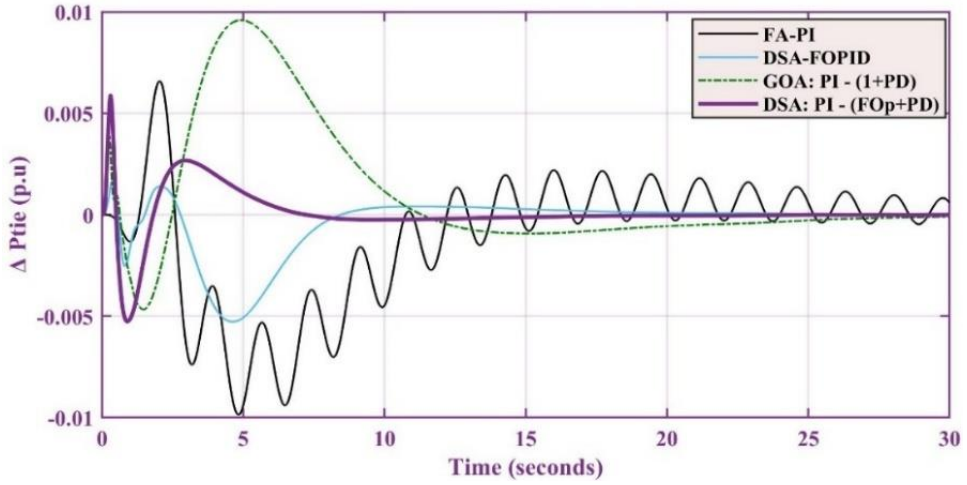


**Figure 11.** Tie-line power exchange response at 2.5% load change.

All the results are compiled in Table 3, where a better understanding about the achieved results can be observed.

**Table 3.** Response of controllers in area-1 and area-2 at 1% and 2.5%.

| Controllers | Area-1 | | | | | | Area-2 | | | | | |
|---|---|---|---|---|---|---|---|---|---|---|---|---|
| | 1% | | | 2.5% | | | 1% | | | 2.5% | | |
| | S.T (s) | U.S (Hz) | O.S (Hz) | S.T (s) | U.S (Hz) | O.S (Hz) | S.T (s) | U.S (Hz) | O.S (Hz) | S.T (s) | U.S (Hz) | O.S (Hz) |
| Proposed | 2.82 | 0 | 0.042 | 4.120 | 0.046 | 0.063 | 3.13 | 0 | 0.093 | 3.608 | 0.144 | 0.054 |
| DSA-FOPID [20] | 3.02 | 0 | 0.188 | 4.331 | 0.141 | 0.180 | 5.08 | 0 | 1.833 | 4.423 | 0.186 | 0.175 |
| GWO: PI-PD [19] | 6.240 | 0 | 0.045 | 6.031 | 0.035 | 0.061 | 6.731 | 0 | 0.092 | 6.325 | 0.103 | 0.031 |
| FA-PI [7] | 21.6 | 0 | 0.89 | 18.361 | 0.346 | 0.850 | 21.31 | 0 | 0.83 | 19.631 | 0.332 | 0.822 |

The designed controller is further tested by applying varying step load change and efficacy of the controller for area-1 and area-2, and their interconnected power-sharing response is evaluated and discussed. The changing load profile is presented in Figure 12, and the response of the frequency is visualized against the applied load profile in Figures 13–15.

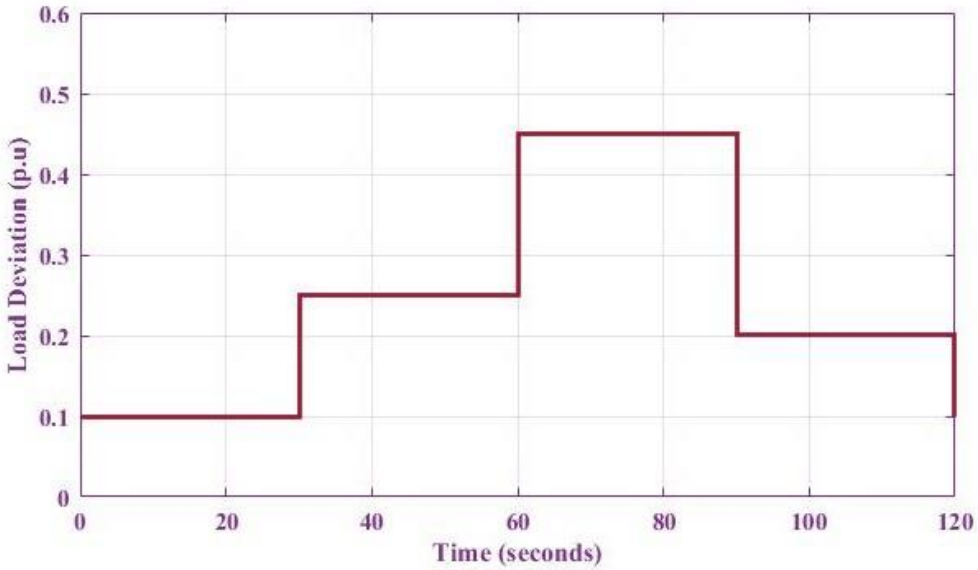


**Figure 12.** Abrupt load deviation presentation.

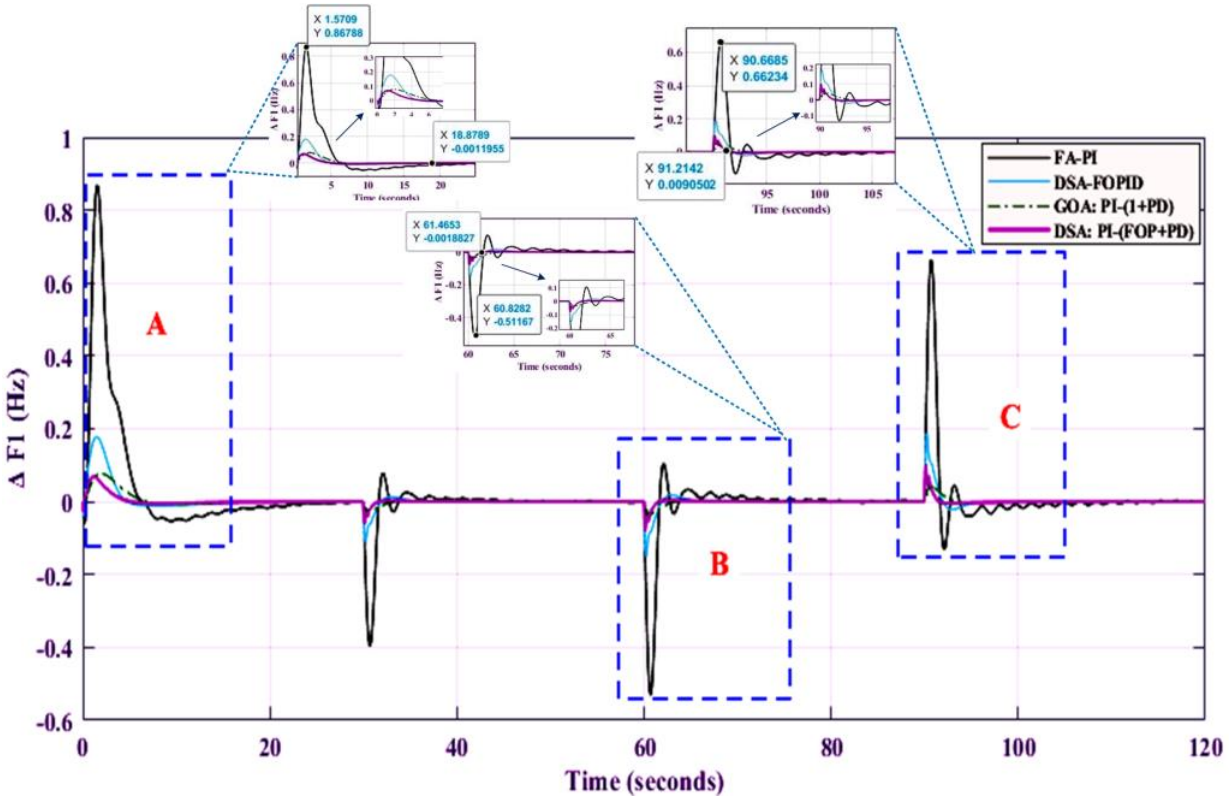


**Figure 13.** Area-1 frequency response.

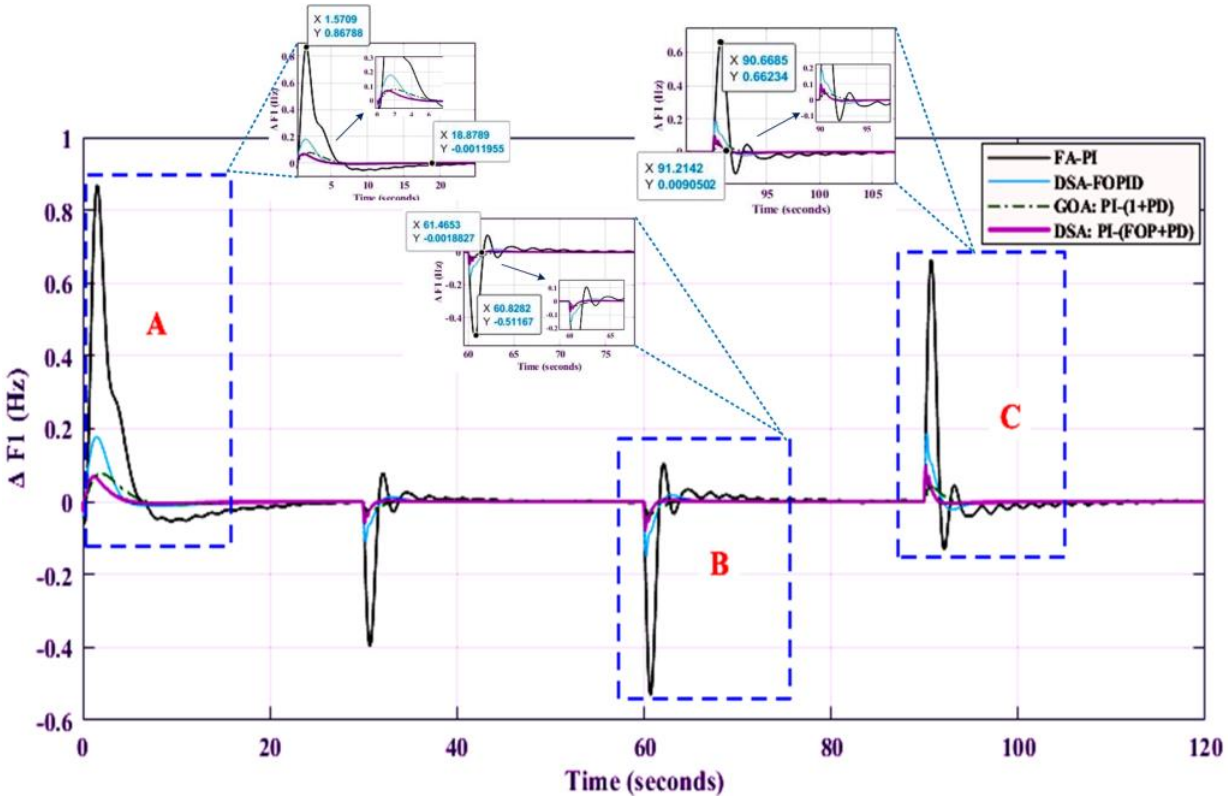


**Figure 14.** Area-2 frequency response.

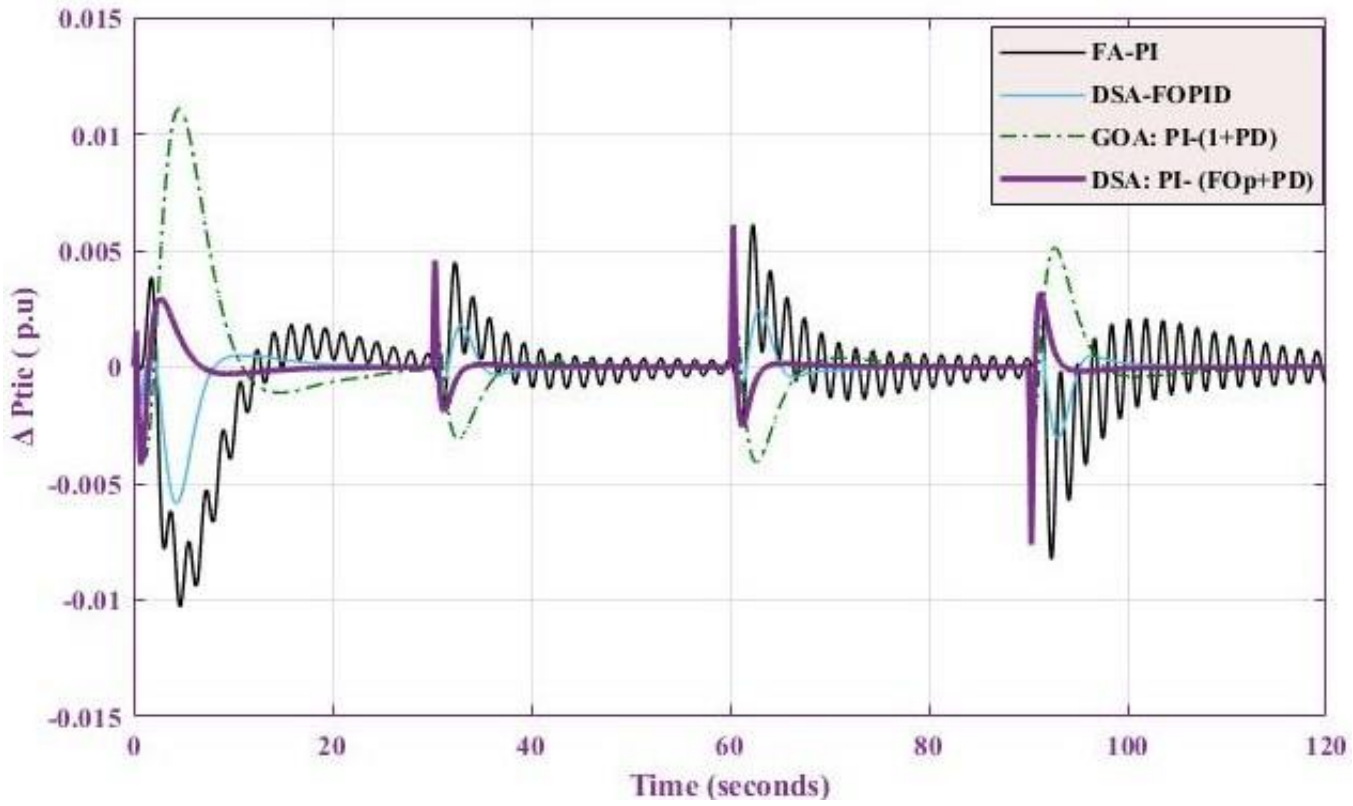


**Figure 15.** Tie-line power sharing.

It is apparent from the results that the designed controller is effectively mitigating the frequency fluctuation in a minimal response time as compared with other controllers. The modified cascaded design with an addition of factor $(\beta)$ expedites the tracking ability by expanding its controlling range.

The power sharing between the interconnected multihybrid power areas is displayed in Figure 15.

Furthermore, the results are compiled in Table 4 at 7% load change, which is the worst-case scenario occurring at 60 s at which a power system can experience a load change.

**Table 4.** Performance of controllers in Area-1 and Area-2 at 7% load change.

| Controllers | Area-1 | | | Area-2 | | |
|---|---|---|---|---|---|---|
| | **S.T (s)** | **U.S (Hz)** | **O.S (Hz)** | **S.T (s)** | **U.S (Hz)** | **O.S (Hz)** |
| DSA: PI-(FOp+PD) | 1.465 | 0.0362 | 0 | 1.501 | 0.107 | 0 |
| DSA-FOPID [20] | 4.721 | 0.1780 | 0 | 4.809 | 0.168 | 0.002 |
| GWO: PI-PD [19] | 6.213 | 0.0215 | 0 | 3.989 | 0.087 | 0 |
| FA-PI [7] | 19.391 | 0.511 | 0.121 | 20.504 | 0.569 | 0.108 |

Further investigation about the performance of the designed controller is tested by introducing a communication time delay in the system at the input side of the controller. The response of the DSA: PI $-$ $(FO_p + PD)$ is exhibited in Figures 16–18 that proclaim the optimal performance of the system by fast convergence to the reference frequency with minimum oscillations.

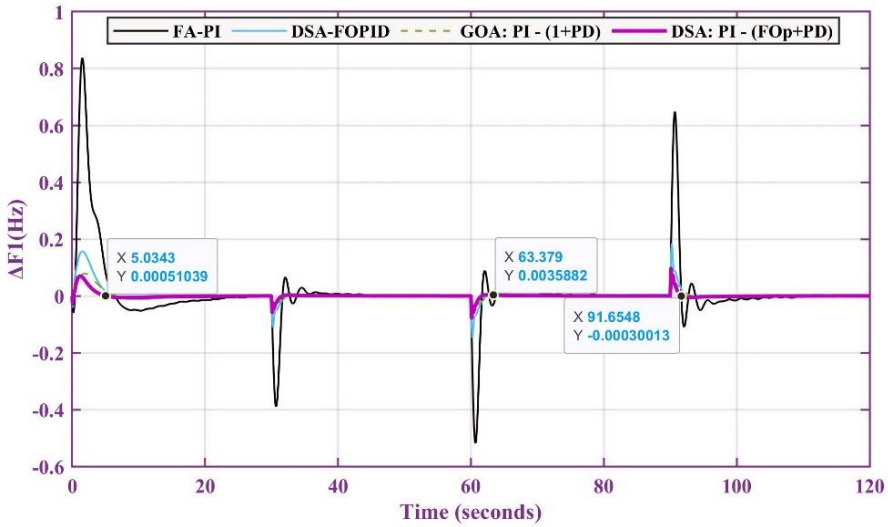


**Figure 16.** Area-1 response with communication delay.

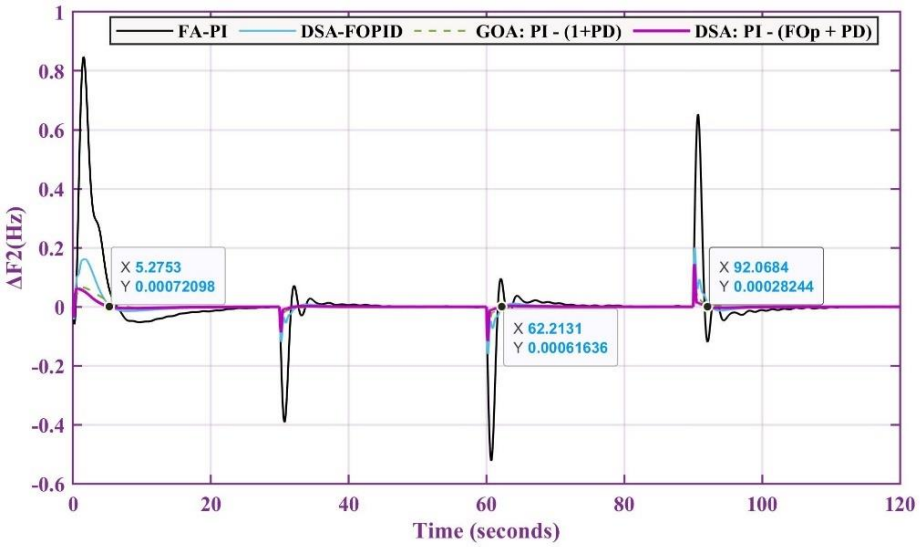


**Figure 17.** Area-2 response with communication delay.

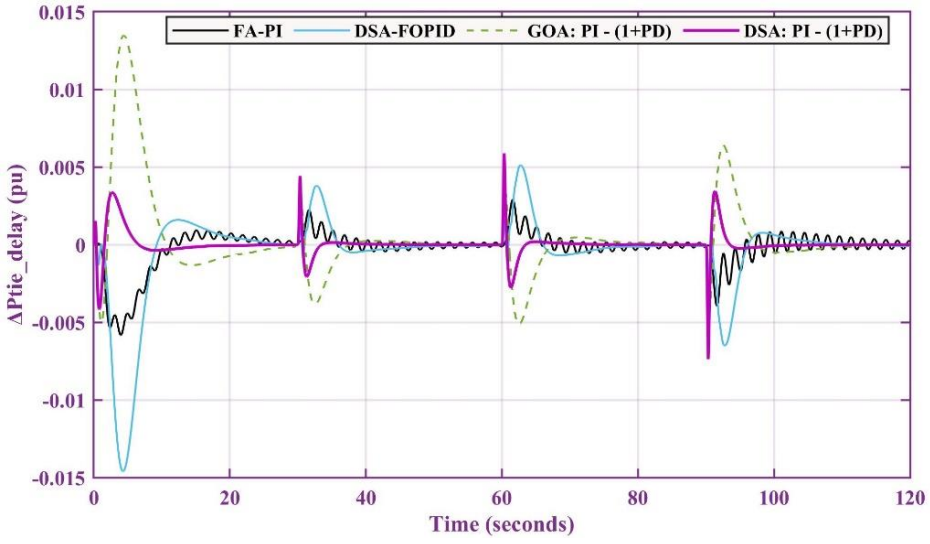


**Figure 18.** Tie-line power exchange response with communication delay.

The results are compiled in Table 5 at 7% load change, which is the worst-case scenario occurring at 60 s at which a power system can experience a load change.

**Table 5.** Communication delay performance of controllers in Area-1 and Area-2 at 7% load change.

| Controllers | Area-1 | | | Area-2 | | |
|---|---|---|---|---|---|---|
| | **S.T (s)** | **U.S (Hz)** | **O.S (Hz)** | **S.T (s)** | **U.S (Hz)** | **O.S (Hz)** |
| DSA: PI-(FOp+PD) | 3.379 | 0.0451 | 0 | 2.213 | 0.151 | 0 |
| DSA-FOPID [20] | 5.181 | 0.185 | 0 | 5.629 | 0.171 | 0 |
| GWO: PI-PD [19] | 6.601 | 0.0221 | 0 | 3.995 | 0.089 | 0 |
| FA-PI [7] | 19.801 | 0.546 | 0.118 | 20.634 | 0.570 | 0.131 |

Furthermore, the performance of the proposed controller is compared with other cutting-edge controllers, i.e., DSA-FOPID, GWO: PI-PD, and FA-PI, in terms of the performance ITAE (objective function) by utilizing Equation (10). The performance of the algorithm is statistically summarized in Table 6.

**Table 6.** Performance analysis of different controllers.

| Controllers | ITAE | | | | |
|---|---|---|---|---|---|
| | $\mathbf{ITAE_{max}}$ | $\mathbf{ITAE_{min}}$ | $\mathbf{ITAE_{avg}}$ | $\mathbf{ITAE_{std}}$ | $\mathbf{T_{ave}}$ **(s)** |
| DSA: PI-(FOp+PD) | 0.0072 | 0.0012 | 0.0023 | 0.0013 | 703.28 |
| DSA-FOPID [20] | 0.0093 | 0.0019 | 0.0038 | 0.0021 | 752.80 |
| GWO: PI-PD [19] | 0.0082 | 0.0015 | 0.0025 | 0.0018 | 729.01 |
| FA-PI [7] | 0.0869 | 0.0056 | 0.024 | 0.0245 | 879.22 |

## 5. Conclusions

The modified cascaded structure is designed for a hybrid power system, where the proposed controller is modified in such a way that it mitigates the frequency oscillation with least settling time with minimum oscillations. The proposed $FO_P$+PD modifies the (1+PD) controller by introducing fractional properties, which improves its tracking efficiency, and the introduction of $FO_P$ $(\beta)$ diversifies its tracking and overall controlling ability. The results signify its robustness by showing abrupt response with minimum settling time. The proposed controller is tested under practically a load-changing scenario where the worst load changes up to 7%, and, under such a case, the designed controller has attained a settling time of 1.465 s and 1.501 s for area-1 and area-2, respectively. Meanwhile, under the communication time delay, the settling time of the proposed controller is 3.379 s and 2.213 s for area-1 and area-2, respectively.

**Author Contributions:** Conceptualization, Writing—original draft, M.M.G. and D.S.; Writing—review & editing, S.M., K.S., I.J. and Y.G. All authors have read and agreed to the published version of the manuscript.

**Funding:** This research received no external funding.

**Data Availability Statement:** Not applicable.

**Conflicts of Interest:** The authors declare no conflict of interest.

## References

1. Dyak, A.A.; Alsafasfeh, Q.; Harb, A. Stability analysis of connected large-scale renewable energy sources into Jordanian national power grid. *Int. J. Ambient. Energy* **2018**, *42*, 1016–1025.
2. Gui, Y.; Blaabjerg, F.; Wang, X.; Bendtsen, J.D.; Yang, D.; Stoustrup, J. Improved DC-Link Voltage Regulation Strategy for Grid-Connected Converters. *IEEE Trans. Ind. Electron.* **2020**, *68*, 4977–4987. [CrossRef]
3. Gao, S.; Zhao, H.; Gui, Y.; Zhou, D.; Blaabjerg, F. An Improved Direct Power Control for Doubly Fed Induction Generator. *IEEE Trans. Power Electron.* **2020**, *36*, 4672–4685. [CrossRef]
4. Khezri, R.; Oshnoei, A.; Oshnoei, S.; Bevrani, H.; Muyeen, S. An intelligent coordinator design for GCSC and AGC in a two-area hybrid power system. *Appl. Soft Comput.* **2019**, *76*, 491–504. [CrossRef]

5. Usman Khan, F.; Gulzar, M.M.; Sibtain, D.; Usman, H.M.; Hayat, A. Variable step size fractional incremental conductance for MPPT under changing atmospheric conditions. *Int. J. Numer. Model. Electron. Netw. Devices Fields* **2020**, *33*, e2765. [CrossRef]
6. Chen, C.; Zhang, K.; Yuan, K.; Gao, Z.; Teng, X.; Ding, Q. Disturbance rejection-based LFC for multi-area parallel interconnected AC/DC system. *IET Gener. Transm. Distrib.* **2016**, *10*, 4105–4117. [CrossRef]
7. Gulzar, M.M.; Iqbal, M.; Shahzad, S.; Muqeet, H.A.; Shahzad, M.; Hussain, M.M. Load Frequency Control (LFC) Strategies in Renewable Energy-Based Hybrid Power Systems: A Review. *Energies* **2022**, *15*, 3488. [CrossRef]
8. Bayu, E.S.; Khan, B.; Ali, Z.M.; Alaas, Z.M.; Mahela, O.P. Mitigation of Low-Frequency Oscillation in Power Systems through Optimal Design of Power System Stabilizer Employing ALO. *Energies* **2022**, *15*, 3809. [CrossRef]
9. Hanan; Muhammad; Ai, X.; Javed, M.Y.; Gulzar, M.M.; Ahmad, S. A two-stage algorithm to harvest maximum power from photovoltaic system. In Proceedings of the 2018 2nd IEEE Conference on Energy Internet and Energy System Integration (EI2), Beijing, China, 20–22 October 2018; pp. 1–6.
10. Qi, B.; Hasan, K.N.; Milanovic, J.V. Identification of Critical Parameters Affecting Voltage and Angular Stability Considering Load-Renewable Generation Correlations. *IEEE Trans. Power Syst.* **2019**, *34*, 2859–2869. [CrossRef]
11. Kim, C.; Gui, Y.; Chung, C.C. Coordinated wind power plant control for frequency support under wake effects. In Proceedings of the 2015 IEEE Power & Energy Society General Meeting, Denver, CO, USA, 26–30 July 2015; pp. 1–5.
12. Shahid, K.; Nainar, K.; Olsen, R.L.; Iov, F.; Lyhne, M.; Morgante, G. On the Use of Common Information Model for Smart Grid Applications—A Conceptual Approach. *IEEE Trans. Smart Grid* **2021**, *12*, 5060–5072. [CrossRef]
13. Shahid, K.; Altin, M.; Mikkelsen, L.M.; Olsen, R.L.; Iov, F. ICT Based Performance Evaluation of Primary Frequency Control Support from Renewable Power Plants in Smart Grids. *Energies* **2018**, *11*, 1329. [CrossRef]
14. Lee, W.-G.; Nguyen, T.-T.; Kim, H.-M. Multiagent-Based Distributed Coordination of Inverter-Based Resources for Optimal Operation of Microgrids Considering Communication Failures. *Energies* **2022**, *15*, 3736. [CrossRef]
15. Abd-Elazim, S.M.; Ali, E.S. Firefly algorithm-based load frequency controller design of a two-area system composing of PV grid and thermal generator. *Electr. Eng.* **2018**, *100*, 1253–1262. [CrossRef]
16. Gulzar, M.M.; Rizvi, S.T.H.; Javed, M.Y.; Sibtain, D.; Din, R.S.U. Mitigating the Load Frequency Fluctuations of Interconnected Power Systems Using Model Predictive Controller. *Electronics* **2019**, *8*, 156. [CrossRef]
17. Sahin, S.; Ayasun, S. Stability region in the parameter space of PI controller for a single-area load frequency control system with time delay. *IEEE Trans. Power Syst.* **2015**, *31*, 829–830.
18. Paliwal, N.; Srivastava, L.; Pandit, M. PSO-Based PID Controller Designing for LFC of Single Area Electrical Power. In *Nature Inspired Optimization for Electrical Power System*; Springer: Singapore, 2020; pp. 43–54.
19. Abdelaziz, A.Y.; Ali, E.S. Load frequency controller design via artificial cuckoo search algorithm. *Electr. Power Compon. Syst.* **2016**, *44*, 90–98. [CrossRef]
20. Nguyen, G.N.; Jagatheesan, K.; Ashour, A.S.; Anand, B.; Dey, N. Ant colony optimization based load frequency control of multi-area interconnected thermal power system with governor dead-band nonlinearity. In *Smart Trends in Systems, Security and Sustainability*; Springer: Singapore, 2018; pp. 157–167.
21. Dhillon, S.S.; Lather, J.S.; Wang, G.-G.; Kaur, P.; Kumar, L. Monarch butterfly optimized control with robustness analysis for grid tied centralized and distributed power generations. *J. Ambient Intell. Humaniz. Comput.* **2020**, *13*, 3595–3608. [CrossRef]
22. Jagatheesan, K.; Anand, B.; Samanta, S. Flower Pollination Algorithm Tuned PID Controller for Multi-source Interconnected Multi-area Power System. *Appl. Flower Pollinat. Algorithm Its Var.* **2021**, 221–239.
23. Padhy, S.; Panda, S. A hybrid stochastic fractal search and pattern search technique based cascade PI-PD controller for automatic generation control of multi-source power systems in presence of plug in electric vehicles. *CAAI Trans. Intell. Technol.* **2017**, *2*, 12–25. [CrossRef]
24. Jayabarathi, T.; Raghunathan, T.; Gandomi, A.H. The bat algorithm, variants and some practical engineering applications: A review. *Nat.-Inspired Algorithms Appl. Optim.* **2018**, *744*, 313–330.
25. Mishra, S.; Gupta, S.; Yadav, A. Design and application of controller based on sine-cosine algorithm for load frequency control of power system. In *International Conference on Intelligent Systems Design and Applications*; Springer: Cham, Switzerland, 2018; pp. 301–311.
26. Satapathy, P.; Debnath, M.K.; Mohanty, P.K. Design of PD-PID controller with double derivative filter for frequency regulation. In Proceedings of the 2018 2nd IEEE International Conference on Power Electronics, Intelligent Control and Energy Systems (ICPEICES), Delhi, India, 22–24 October 2018; pp. 1142–1147.
27. Latif, A.; Hussain, S.S.; Das, D.C.; Ustun, T.S. Double stage controller optimization for load frequency stabilization in hybrid wind-ocean wave energy based maritime microgrid system. *Appl. Energy* **2021**, *282*, 116171. [CrossRef]
28. Emre, Ç. Design of new fractional order PI–fractional order PD cascade controller through dragonfly search algorithm for advanced load frequency control of power systems. *Soft Comput.* **2021**, *25*, 1193–1217.
29. Oladipo, S.; Sun, Y.; Wang, Z. Application of a New Fusion of Flower Pollinated With Pathfinder Algorithm for AGC of Multi-Source Interconnected Power System. *IEEE Access* **2021**, *9*, 94149–94168. [CrossRef]
30. Khokhar, B.; Dahiya, S.; Singh Parmar, K.P. A robust Cascade controller for load frequency control of a standalone microgrid incorporating electric vehicles. *Electr. Power Compon. Syst.* **2020**, *48*, 711–726. [CrossRef]

31. Gulzar, M.M.; Sibtain, D.; Murtaza, A.F.; Murawwat, S.; Saadi, M.; Jameel, A. Adaptive fuzzy based optimized proportional-integral controller to mitigate the frequency oscillation of multi-area photovoltaic thermal system. *Int. Trans. Electr. Energy Syst.* **2021**, *31*, e12643. [CrossRef]
32. Chowdhury, A.H.; Asaduz-Zaman, M. Load frequency control of multi-microgrid using energy storage system. In *8th International Conference on Electrical and Computer Engineering*; IEEE: Dhaka, Bangladesh, 2014; pp. 548–551.
33. Iqbal, M.; Gulzar, M.M. Mastger-slave design for frequency regulation in hybrid power system under complex environment. *IET Renew. Power Gener.* **2022**, 1–17.